

# Compact lattice QED with Wilson fermions <sup>†</sup>

A. Hoferichter <sup>1</sup>, V.K. Mitrjushkin <sup>1 ‡</sup>, M. Müller-Preussker <sup>1</sup>,  
T. Neuhaus <sup>2</sup> and H. Stüben <sup>3</sup>

<sup>1</sup> *Humboldt-Universität, Institut für Physik, 10099 Berlin, Germany*

<sup>2</sup> *Universität Bielefeld, Fakultät für Physik, 33615 Bielefeld, Germany*

<sup>3</sup> *Konrad-Zuse-Zentrum für Informationstechnik Berlin, 10711 Berlin, Germany*

## Abstract

We study the phase structure and the chiral limit of  $4d$  compact lattice QED with Wilson fermions (both dynamical and quenched). We use the standard Wilson gauge action and also a modified one suppressing lattice artifacts. Different techniques and observables to locate the chiral limit are discussed.

---

<sup>†</sup>Work supported by the Deutsche Forschungsgemeinschaft under research grant Mu 932/1-2

<sup>‡</sup>Permanent adress: Joint Institute for Nuclear Research, Dubna, Russia

# 1 Introduction

QED is commonly recognized to be a very successful quantum field theory. Nevertheless, despite the excellent agreement found between the perturbative predictions of the theory and some experimental results, QED is still a poorly understood theory. The most unsatisfactory feature of QED is the so-called Landau pole problem. When a test charge is added to the vacuum of QED, pair creation around this charge totally screens it and the resulting charge observed at large distances is zero. That means that QED becomes 'trivial'. Formally we need a cutoff to make it nontrivial. Lattice (nonperturbative) QED is supposed to resolve this problem.

There are different lattice formulations of QED (e.g., with compact or non-compact treatment of the gauge field degrees of freedom and with staggered or Wilson fermions, respectively) possibly not belonging to the same class of universality. If so, on a physical ground one has to decide which version of QED is realized in nature. Old, i.e. experimentally well-established physical results should finally be reproduced (at least qualitatively) from lattice computations.

If we consider QED as arising from a subgroup of a non-abelian (e.g., grand unified) gauge theory, then we are led to a compact treatment, a point of view we want to adopt throughout this work. Concerning the fermion degrees of freedom we are dealing with Wilson fermions [1, 2], which – to our knowledge – have not yet been thoroughly investigated in case of QED.

In a theory with Wilson fermions the chiral symmetry is broken explicitly. Presumably, it can be restored by fine-tuning the parameters in the continuum limit. But, for nonzero lattice spacing we can expect only a partial symmetry restoration at some value of the hopping parameter  $\kappa_c \equiv \kappa_c(\beta)$  by cancellation of the Wilson mass term with the ordinary mass term in certain vertex functions at zero momentum [3, 4]. If so, we can approach the continuum limit and the chiral symmetry restoration along the line  $\kappa_c(\beta)$ . It is another question, whether there the chiral symmetry becomes explicitly realized or spontaneously broken.

It is worthwhile to note that QED can also serve as a 'toy' model of QCD for the study of, e.g., the chiral transition. Therefore, even the confinement phase of QED is of interest, since the fermionic observables should behave similar to the case of QCD.

In this work we investigate the phase structure of  $4d$  lattice QED with special emphasis on the chiral limit. We consider the standard Wilson action (WA) and a modified one (MA) which is derived from WA by introducing suppression terms for lattice artifacts into the gauge action. We discuss different techniques to establish the chiral limit. On the one hand they are based on the convergence rate of the conjugate gradient algorithm to invert the fermion matrix, on the other hand they use observables sensitive to the occurrence of zero modes. Some preliminary results have been published in [5]. These techniques are applicable to lattice QCD studies with Wilson fermions as well.

We concentrate on the study of gauge invariant observables as a first step, be-

cause for gauge variant quantities such as the photon and fermion correlators one has to take care of gauge fixing ambiguities [6, 7, 8].

The organization of the paper is as follows. In the second section we define both actions and the fermionic gauge invariant 'order parameters' which we calculated. The third section is devoted to the discussion of the matrix inversion. The results of our calculations for the quenched fermions and for the dynamical fermions are presented in the fourth and fifth sections, respectively. The last section is reserved for the conclusions and the outlook.

## 2 Actions and observables

The standard Wilson lattice action  $S_{WA}(U, \bar{\psi}, \psi)$  for 4d compact  $U(1)$  gauge theory (QED) is

$$S_{WA} = S_G(U) + S_F(U, \bar{\psi}, \psi). \quad (1)$$

In eq.(1)  $S_G(U)$  is the plaquette (Wilson) action for the pure gauge  $U(1)$  theory

$$S_G(U) = \beta \cdot \sum_P (1 - \cos \theta_P), \quad (2)$$

where  $\beta = 1/g_{bare}^2$ , and  $U_{x\mu} = \exp(i\theta_{x\mu})$ ,  $\theta_{x\mu} \in (-\pi, \pi]$  are the field variables defined on the links  $l = (x, \mu)$ . Plaquette angles  $\theta_P \equiv \theta_{x;\mu\nu}$  are given by  $\theta_{x;\mu\nu} = \theta_{x;\mu} + \theta_{x+\hat{\mu};\nu} - \theta_{x+\hat{\nu};\mu} - \theta_{x;\nu}$ .

The fermionic part of the action  $S_F(U, \bar{\psi}, \psi)$  is

$$\begin{aligned} S_F &= \sum_{f=1}^{N_f} \sum_{x,y} \sum_{s,s'=1}^4 \bar{\psi}_x^{f,s} \mathcal{M}_{xy}^{ss'} \psi_y^{f,s'} \equiv \bar{\psi} \mathcal{M} \psi, \\ \mathcal{M} &\equiv \hat{1} - \kappa \cdot Q(U), \\ Q_{xy}^{ss'} &= \sum_{\mu} \left[ \delta_{y,x+\hat{\mu}} \cdot (\hat{1} - \gamma_{\mu})_{ss'} \cdot U_{x\mu} + \delta_{y,x-\hat{\mu}} \cdot (\hat{1} + \gamma_{\mu})_{ss'} \cdot U_{x-\hat{\mu},\mu}^{\dagger} \right], \end{aligned} \quad (3)$$

where  $\mathcal{M}$  is Wilson's fermionic matrix,  $N_f$  is the number of flavours (we take  $N_f = 2$  for the case of dynamical fermions), and  $\kappa$  is the hopping parameter.

In our calculations we also used the modified (compact) action  $S_{MA}$  with Wilson fermions

$$S_{MA} = S_{WA}(U) + \delta S_G(U), \quad (4)$$

where the additional term  $\delta S_G$  is introduced to suppress some lattice artifacts, i.e., monopoles and negative plaquettes. The notion of (DeGrand–Toussaint) monopoles

can be introduced as follows [9] : the plaquette angle is splitted into two parts

$$\theta_P = \bar{\theta}_P + 2\pi n_P, \quad \bar{\theta}_P \in (-\pi, \pi], \quad n_P = 0, \pm 1, \pm 2, \quad (5)$$

where  $\bar{\theta}_P$  is associated with the (gauge-invariant) 'electromagnetic' flux through the plaquette and  $n_P$  is the number of Dirac strings passing through it. The monopole charge within an elementary  $3d$  cube  $c$  is defined as the net number of Dirac strings passing through the surface of  $c$  :

$$K_c = \frac{1}{2\pi} \sum_{P \in \partial c} \bar{\theta}_P = - \sum_{P \in \partial c} n_P \quad (6)$$

where the correct mutual orientation of the plaquettes has to be taken into account. The suppression term in eq. (4) can then be written as

$$\delta S_G(U) = \lambda_K \cdot \sum_c |K_c| + \lambda_P \cdot \sum_P (1 - \text{sign}(\cos \theta_P)) \quad (7)$$

with  $\lambda_K$  and  $\lambda_P$  as 'chemical potentials' controlling the suppression rate of the corresponding artifacts. We have chosen  $(\lambda_K, \lambda_P) = (\infty, \infty)$  in order to obtain maximal suppression of monopoles and negative plaquette values. Then for the quantized theory the suppression terms can easily be rewritten as Kronecker deltas in the measure of the functional integral.

In the case of the pure gauge  $U(1)$  theory the complete suppression of monopoles removes the phase transition at  $\beta_0 \simeq 1.0$  [10, 11], and a unique Coulomb phase at positive  $\beta$ 's appears [11]. For staggered fermions no chiral transition is observed as shown in [12]. The additional suppression of negative plaquettes drastically improves the overlap with the lowest state, at least, for the case of the photon [11].

It is known, that at least in the strong coupling region for the standard Wilson action (in the confinement phase) the ordinary mass term and the Wilson mass term cancel within the pseudoscalar mass  $m_P$  at some  $\kappa = \kappa_c(\beta)$ , so that quadratic terms in the effective potential vanish for the pseudoscalar field, and  $\kappa_c = 0.25$  at  $\beta = 0$  [4].

In the weak coupling range (Coulomb phase) perturbative calculations indicate that the mass of the fermion becomes equal to zero along the line  $\kappa_c(\beta)$  (for the free field theory  $\kappa_c = 0.125$ ) [3].

Besides the average plaquette  $\langle P \rangle$  we calculated the following fermionic observables

$$\langle \bar{\psi}\psi \rangle = \frac{1}{4V} \cdot \langle \text{Tr}(\mathcal{M}^{-1}) \rangle_G, \quad (8)$$

$$\langle \bar{\psi}\gamma_5\psi \rangle = \frac{1}{4V} \cdot \langle \text{Tr}(\gamma_5\mathcal{M}^{-1}) \rangle_G, \quad (9)$$

$$\langle \Pi \rangle = \frac{1}{4V} \cdot \langle \text{Tr}(\mathcal{M}^{-1}\gamma_5\mathcal{M}^{-1}\gamma_5) \rangle_G, \quad (10)$$

where  $\langle \rangle_G$  stands for averaging over gauge configurations which in presence of dynamical fermions includes the fermionic determinant.  $V = L^4$  is the number of sites. The advantage of the order parameter in eq.(10) – the 'pion norm' [13] – is that it appears to be a very sensitive observable in the 'critical' region. This can be understood by considering the spectral representation of the fermionic order parameters. Let  $f_n \equiv f_n(s, x)$  be the eigenvectors of  $\mathcal{M}$  with eigenvalues  $\lambda_n$ , and  $g_n \equiv g_n(s, x)$  be the eigenvectors of  $\gamma_5 \mathcal{M}$  with eigenvalues  $\mu_n$  :

$$\mathcal{M}f_n = \lambda_n \cdot f_n, \quad \gamma_5 \mathcal{M}g_n = \mu_n \cdot g_n. \quad (11)$$

Then one can easily obtain a spectral representation of the fermionic order parameters :

$$\begin{aligned} \langle \bar{\psi}\psi \rangle &= \frac{1}{4V} \left\langle \sum_n \frac{1}{\lambda_n} \right\rangle_G, & \langle \bar{\psi}\gamma_5\psi \rangle &= \frac{1}{4V} \left\langle \sum_n \frac{1}{\mu_n} \right\rangle_G, \\ \langle \Pi \rangle &= \frac{1}{4V} \left\langle \sum_n \frac{1}{\mu_n^2} \right\rangle_G. \end{aligned} \quad (12)$$

Evidently, an eigenstate of  $\mathcal{M}$  with eigenvalue zero is also eigenstate of  $\gamma_5 \mathcal{M}$ . So, the presence of configurations which belong to zero eigenvalues of  $\mathcal{M}$  also gives rise to poles in  $\Pi$  (for more properties of the fermion matrix see, e.g. [14]).

It is commonly expected that close to  $\kappa_c$  the minimal eigenvalue  $|\lambda_{min}|^2$  of  $\mathcal{M}^\dagger \mathcal{M}$  is small and

$$|\lambda_{min}|^2 \sim \left( 1 - \frac{\kappa}{\kappa_c} \right)^2. \quad (13)$$

Therefore, the appearance of small eigenvalues  $\lambda_i \sim 0$  can be a good indicator for the chiral transition. For more discussion on this point for the Wilson action see, e.g., [15, 16] and references therein.

In our calculations we have chosen periodic boundary conditions for fermions in all four directions. It is worthwhile to notice here that in the case of quenched fermions the choice between periodic and antiperiodic boundary conditions is irrelevant. Indeed, the change of the sign of all, say, time-like links in the 'last' time slice does not change the gauge action, but this corresponds to the interchange of periodic and antiperiodic boundary conditions for fermions [17].

In order to extract information about the photon mass we have measured the photon plaquette–plaquette correlator at non-vanishing momenta and for several values of the coupling parameters (see [18, 11]).

### 3 Matrix inversion

The inversion of the fermionic matrix  $\mathcal{M} \equiv \hat{1} - \kappa \cdot Q(U)$  defined in eq.(3) is equivalent to solving the matrix equation

$$\mathcal{M} \cdot X = \varphi . \quad (14)$$

for any given 'input'-vector  $\varphi$ .

One of the most popular methods is the conjugate gradient method (see, e.g., [19, 20] and references therein). This is an iterative method to solve systems of linear equations  $D \cdot X = \varphi$ , where  $D$  is a hermitian  $n \times n$  matrix and  $\varphi$  is an input vector. The convergence of the conjugate gradient (cg) method is controlled by the condition number  $\xi \equiv \lambda_{max}/\lambda_{min}$ , where  $\lambda_{max}$  and  $\lambda_{min}$  are the maximal and minimal eigenvalues of  $D$  ( $D = \mathcal{M}^\dagger \mathcal{M}$  in this case). We observed for our standard cg-method that at a large enough number of iteration steps  $N_{cg}$  the average residue  $\langle R \rangle \equiv \langle R \rangle(N_{cg})$  behaves as

$$\begin{aligned} \langle R \rangle &= C \cdot \exp(-\alpha \cdot N_{cg}) \quad \text{for } N_{cg} > N_0, \\ \alpha &= \ln \frac{\sqrt{\xi} + 1}{\sqrt{\xi} - 1} \end{aligned} \quad (15)$$

*independently of the distribution of eigenvalues  $\lambda_i$  provided  $n$  is large enough.* This kind of functional dependence of  $\alpha$  on  $\xi$  was analytically obtained for some other gradient methods (e.g. Chebyshev methods) [20]. To check the behaviour (15) we generated  $D$  with different (uniform, gaussian, double-peaked,...) distributions of eigenvalues and given  $\lambda_{min}$  and  $\lambda_{max}$ . The components of the input-vector  $\varphi$  were chosen randomly with gaussian distributions.

In Fig.1 we show the dependence of the average (normalized to unity at  $N_{cg} = 1$ ) residue  $\langle R \rangle$  on  $N_{cg}$  for a gaussian distribution of eigenvalues  $\lambda_i$  of the matrix  $D$  in the interval  $[\lambda_{min}; \lambda_{max}]$  as an illustration. Broken lines correspond to the behaviour  $\exp(-\alpha \cdot N_{cg})$ . One can see that after some steps  $N_{cg} > N_0$  eq.(15) works very well. The behaviour practically does not depend on the choice of the initial vector  $X_0$ : we checked this for a gaussian distribution of the components  $X_0(i)$  and for different 'ordered starts' (e.g.,  $X_0(1) = 1$ ,  $X_0(i) = 0$  at  $i > 1$ ). The parameters  $N_0$  and  $C$  depend on the distribution of  $\lambda_i$ .

This observation gives the possibility to use the convergence of the cg-method to estimate  $\kappa_c$ . This estimation, however, is biased because of the dependence of the parameters  $N_0$  and  $C$  on the distribution of eigenvalues.

Obviously, the fermion matrix inversion is the most time consuming step in the numerical work. Therefore, a maximal improvement of the convergence of the conjugate gradient algorithm is highly important, in particular near  $\kappa_c$ . We have achieved considerable improvement by the use of preconditioning methods, e.g., polynomial preconditioning [21] plus 'even-odd decomposition' [22, 23]. Furthermore, the appropriate choice of the start vector  $X_0$  allows to speed up the procedure additionally:

$$X_0 = \left[ \hat{1} + \sum_{l=1}^{l_0} \kappa^l \cdot Q^l \right] \cdot \varphi , \quad (16)$$

where  $l_0$  is some integer depending on  $\kappa$ . For smaller  $\kappa$ -values (far enough from  $\kappa_c$ ) the hopping parameter expansion (16) with large enough  $l_0$  already represents a good approximation of the solution we search for. This approximation is even less time consuming than a combined application with the cg-method.

## 4 Quenched fermions

The quenched approximation of the theory can serve to provide very useful information about the behaviour of the fermionic order parameters and to develop the numerical tools. Its comparison with the full theory is instructive for the elucidation of the influence of the fermionic determinant. Moreover, it has the advantage to be less time consuming than the full theory.

As it was already mentioned the phase transition at  $\beta_0 \simeq 1.0$  disappears by suppressing lattice artifacts, and the quenched modified theory has only one phase for nonnegative  $\beta$ 's : the Coulomb phase. Qualitatively, the behaviour of the order parameters we measured in the modified theory MA at  $\beta \geq 0$  turned out to be the same as in the standard theory WA within the Coulomb phase ( $\beta > \beta_0$ ).

Let us now discuss the possibility to estimate  $\kappa_c(\beta)$  in the Coulomb phase based on the convergence of the cg-method. It follows from the discussion in the previous section that for the inversion of  $\mathcal{M}^\dagger \mathcal{M}$  the number of cg-iterations required for the convergence to some small  $R \leq \epsilon$  will behave as  $\langle N_{cg}^{-1} \rangle \sim 1 - \kappa/\kappa_c$  as long as  $N_{cg} \gg N_0$  and  $\kappa \sim \kappa_c$ . Therefore, the study of the dependence  $\langle N_{cg}^{-1} \rangle(\kappa)$  for different lattice sizes  $L$  (at fixed coupling  $\beta$ ) can give a rather reliable estimate of  $\kappa_c$ . Fig.2a represents the dependence of  $\langle N_{cg}^{-1} \rangle$  on  $\kappa$  at  $\beta = 1.1$  (Coulomb phase) for quenched WA (qWA) for different  $V = L^4$  up to  $20^4$ . By linear extrapolation  $\langle N_{cg}^{-1} \rangle \rightarrow 0$  one can obtain reasonable estimates of  $\kappa_c$ , which, as we shall see, are consistent with that obtained by other methods. The volume dependence becomes weaker with increasing  $L$ . With increasing matrix size  $n = 4L^4$  also the variance of  $N_{cg}$  with respect to different statistical configurations decreases. An absolutely similar dependence of  $\langle N_{cg}^{-1} \rangle$  on  $\kappa$  we observed for the modified theory MA at different values of the gauge coupling.<sup>1</sup>

The comparison of the two theories WA and MA at  $\beta = 1.1$  (both in the Coulomb phase) shows that the difference in the convergence is rather small, and the estimated values of  $\kappa_c$  are close to each other. Therefore, the influence of lattice artifacts in WA is already small at this value of the coupling. With increasing  $\beta$  the estimated value of  $\kappa_c(\beta)$  shows a weak dependence on  $\beta$ .

Figs.2b,c show the dependence of  $\langle N_{cg}^{-1} \rangle$  on the inverse lattice size  $L^{-1}$  at various values of  $\kappa$  in the case of the quenched standard Wilson action at  $\beta = 1.1$  (b) and the quenched modified action (qMA) at  $\beta = 0.8$  (c) respectively. For this dependence we again see no qualitative difference between Wilson action in the

---

<sup>1</sup>In the confinement phase of WA the number of required cg-iterations is highly increased and one obtains even better estimates of  $\kappa_c$  than in the Coulomb phase.

Coulomb phase and the modified theory and it appears to be

$$\langle N_{cg}^{-1} \rangle_L = \langle N_{cg}^{-1} \rangle_\infty + \frac{C(\kappa)}{L} . \quad (17)$$

Time histories of different observables (e.g.,  $\bar{\psi}\psi$ ,  $\bar{\psi}\gamma_5\psi$ ,  $\Pi$ ) can give a signal of approaching  $\kappa_c$ . The appearance of sharp peaks in their time histories at distinct values of  $\beta$  and  $\kappa$  testifies the appearance of small eigenvalues of the fermionic matrix  $\mathcal{M}$  and, presumably, could be interpreted as approaching the chiral limit.

Fig.3 shows the time histories of the pion norm  $\Pi$  at  $\beta = 0$  for the standard Wilson gauge action (confinement phase) at different  $\kappa$ 's. Strong coupling arguments predict a 'critical' value of  $\kappa$  at  $\kappa_c = 0.25$ . Indeed, one can see that below  $\kappa_c$  time histories are rather 'smooth' and do not show any evidence for peaks. The fluctuations become more pronounced with increasing  $\kappa$ , and finally at  $\kappa_c \sim 0.25$  sharp spikes appear. It is interesting to note that at  $\kappa > \kappa_c$  these spikes do not disappear but instead become even stronger. With increasing  $\beta$  (but at  $\beta < \beta_0$ ) time histories have a similar structure with the only difference that the spikes appear at somewhat smaller values of the Wilson coupling. Thus, e.g.,  $\kappa_c(\beta = 0.8) < \kappa_c(\beta = 0)$ . The time histories of  $\bar{\psi}\psi$  and  $\bar{\psi}\gamma_5\psi$  look similar; here the spikes have a smaller order of magnitude in accordance with the spectral representations.

On the contrary at  $\beta > \beta_0$  for Wilson action (i.e., in the Coulomb phase) the form of the time histories drastically changes (Fig.4). We do not find peaks of comparable amplitude ( $\sim 10^4$ ) but, nevertheless, in a 'critical' region of  $\kappa$ , the histories show up stronger fluctuations than at smaller or *larger* values of the Wilson coupling. Taking into account that for every configuration the pion norm  $\Pi$  is the arithmetic average of  $4 \cdot L^4$  terms corresponding to contributions of  $4 \cdot L^4$  eigenvalues one can conclude that rather small eigenvalues occurred. A similar picture as in the latter case also holds for the modified gauge action.

The increase of fluctuations near  $\kappa_c$  can be best represented by the statistical variances of the observables discussed, especially the variance of  $\Pi$  should be most sensitive. The value which we call (renormalized) variance  $\sigma^2(\Pi)$  is defined as follows

$$\sigma^2(\Pi) = \frac{V}{4^4} \cdot \frac{1}{N} \sum_i^N (\Pi_i - \bar{\Pi})^2, \quad \bar{\Pi} \equiv \frac{1}{N} \sum_i^N \Pi_i \quad (18)$$

where  $\Pi_i$  is the value of  $\frac{1}{4V} \cdot \sum_{xy} \text{Sp}(\mathcal{M}_{xy}^{-1} \gamma_5 \mathcal{M}_{yx}^{-1} \gamma_5)$  for the  $i^{th}$  configuration and  $N$  is the number of measurements. ('Sp' denotes the trace with respect to Dirac-indices). This enables us to locate  $\kappa_c(\beta)$  through the maximum of  $\sigma^2(\Pi)$ .

Figs.5a,b show the variance of the pion norm  $\sigma^2(\Pi)$  in case of the quenched Wilson action qWA in the Coulomb phase at  $\beta = 1.1$  (**a**) and for the quenched modified action qMA at  $\beta = 0$  (**b**). In both cases there is a clear signal for the chiral limit or transition at some  $\kappa_c \sim 0.14$  (**a**) and  $\kappa_c \sim 0.135$  for the case (**b**).

For increasing lattice size  $L$  the peak at these values of  $\kappa_c$  becomes more strong and narrow.

Contrary to this the average pion norm  $\langle \Pi \rangle$  itself (see Fig.8a–crosses) was found to have only a very weak size dependence. Moreover,  $\langle \Pi \rangle$  shows for qWA in the Coulomb phase and qMA the same dependence on  $\kappa$  and it is practically independent of  $\beta$  at fixed  $\kappa \leq 0.125$ .

At  $\beta < \beta_0$  in case of the Wilson action (confinement phase) the value  $\sigma^2(\Pi)$  is well defined only *below*  $\kappa_c(\beta)$ . As it can be seen from the time histories for the pion norm the region  $\kappa > \kappa_c(\beta)$  ( $\beta < \beta_0$ ) is 'infested' by the small eigenvalues of the fermionic matrix, so it is practically impossible to define the average pion norm  $\langle \Pi \rangle$  and other fermionic order parameters as well in this region even with high statistics ( 10.000 measurements in our case ).

Based on our quenched data we draw the following phase diagrams in the  $(\beta, \kappa)$ –plane : as already mentioned the quenched WA has a confinement phase for  $\beta < \beta_0$  and a Coulomb phase ( $\beta > \beta_0$ ), and these phases are separated by a 1st or 2nd order transition line at  $\beta_0$  ([28, 29]). Moreover, we have found a 'critical' line  $\kappa = \kappa_c(\beta)$  which decreases from  $\kappa_c(\beta = 0) = 0.25$  to  $\kappa_c(\beta = \infty) = 0.125$ . These lines subdivide the  $(\beta, \kappa)$ –plane into four areas which in the dynamical fermion case are expected to become distinct phases.

The quenched MA has only one Coulomb phase for positive values of  $\beta$ . The behaviour of our observables corresponds to that in case of the Coulomb phase of qWA. We are also able to locate the line  $\kappa = \kappa_c(\beta)$  which extends over the whole  $\beta$ –range ( $\kappa_c(\beta = 0) \sim 0.13$  and  $\kappa_c(\beta = \infty) = 0.125$ ), dividing the phase diagram into two possible phases in the case of full QED.

At  $\beta = 0$  the compact WA and non–compact QED [24, 25] agree because of the common compact coupling of gauge fields to fermions. Since the values of  $\kappa_c(\beta)$  differ for the quenched WA and quenched MA in the extreme strong coupling limit ( $\beta \rightarrow 0$ ) our modified theory MA might have different chiral properties at strong coupling in comparison with the non–compact QED with Wilson fermions (see [24]).

## 5 Dynamical fermions

For the dynamical fermion case (full QED) we investigated the phase structure and the chiral transition for lattice sizes  $4^4$ ,  $6^4$ ,  $8^4$  and  $12^4$ .

We have simulated both actions (standard Wilson and modified) using the Hybrid Monte Carlo algorithm [26]. Throughout our simulations we have used  $N = 20$  molecular dynamics steps followed by an acceptance/rejectance decision at the end of each trajectory. The length of the trajectories was chosen for most of our runs to be  $N\delta\tau$  equal to unity, resulting into acceptance rates of about 95 % at the considered coupling values. At a few values of the couplings we have considered several stepsize values  $\delta\tau$  on  $4^4$  lattices, where we estimated integrated autocorrelation times for the plaquette operator from runs of about  $10^3$  trajectories. As

far as we can tell, increasing the length of trajectories up to  $N\delta\tau \approx 3$  does not considerably decrease autocorrelation times, while a further increase leads to small acceptance rates and to a deterioration of the achieved MC statistics.

Concerning the simulations with the modified action (4) we have chosen a unique suppression term  $\delta S_G(U)$  in the form

$$\delta S_G(U) = A \cdot \sum_P \left( 1 + \tanh(B \cos \theta_P) \right), \quad (19)$$

since the Kronecker deltas in the functional integral measure cannot be realized in the molecular dynamics part of the Hybrid Monte Carlo procedure in a straightforward way. With an appropriate choice of the parameters  $A$  and  $B$  ( $B < 0$ ) the term (19) leads to a suppression of negative plaquette values. The parameters in eq. (19) were chosen to be  $A = 10$  and  $B = -10$ . We have monitored the distribution functions of local plaquette values : In Fig.6 we display the distribution function of the local plaquette operator at the same values of couplings with (crosses) and without (dots) suppression term as an example. We see, that this choice of parameters leads to an almost complete suppression of negative plaquette values. Moreover, we made sure that in a simulation with a cold start monopoles never occur.

In the simulations with suppression term the length of the trajectories was chosen to be almost a factor of 10 smaller in order to achieve reasonable acceptance rates of about 90 %. It appears as if the constraint on the action reduces the available phase space considerably and allows only for smaller moves in the Hybrid Monte Carlo algorithm.

Now let us turn to the question how the phase diagrams of the quenched theories given at the end of the previous section are changed when we allow for dynamical fermions.

For the Wilson action WA we expect to have at least one additional 'upper left' and one 'upper right' phase which for simplicity we will refer to as the '4rd' (upper left) and '3rd' (upper right) phases (see Fig10a). We do not consider the question of possible additional phases at larger  $\kappa$ -values [3].

At  $\beta \simeq 1.0$  and  $\kappa < \kappa_1 \sim 0.18$  we observe the same phase transition as in the quenched theory. Thermal cycles and time histories for the average plaquette show a clear signal of metastability at  $\beta$ 's close to  $\beta_0$  and at different  $\kappa < \kappa_1$ . As well as in the quenched case this transition is driven by monopole condensation in the confinement phase. However, there is no such signal for  $\bar{\psi}\psi$ , which remains approximately constant at fixed  $\kappa$  and varying  $\beta$  around  $\beta_0$  as measured at  $\kappa = 0.06, 0.08, 0.10$ . Therefore, at the moment we cannot conclude that there is a first order phase transition in this part of the phase diagram in disagreement with [27]. Probably the metastable states are due to the monopole loops wrapping around the torus.

At  $\beta < \beta_0$  thermal cycles with respect to varying  $\kappa$  showed a typical hysteresis behaviour and a metastability for both : the plaquette and  $\bar{\psi}\psi$ . In Fig.7a we

display the hysteresis loop for  $\bar{\psi}\psi$  at  $\beta = 0.8$ . Furthermore, the abelian monopole density strongly decreases with rising  $\kappa$  (Fig.7b). In both of the figures the full (open) symbols correspond to the runs with decreasing (increasing)  $\kappa$ .

For the standard compact gauge action case we therefore expect a 'horizontal' first order transition line from  $(\beta, \kappa_c) = (\beta_1 \lesssim \beta_0, \kappa_1 \sim 0.18)$  to some  $(\beta, \kappa_c) = (\beta_2 \gtrsim 0.15, \kappa_2 \gtrsim \kappa_1)$ , the latter point assumed to be the 'right-lower corner' of the 4th phase (cf. discussion below). This transition is also driven by monopole condensation in the confinement phase. Yet we do not know what kind of transition line the phase boundary between the 4th and the confinement phase is, i.e. the 'horizontal' line continued from  $(\beta, \kappa_c) = (\beta_2, \kappa_2)$  to the point  $(\beta, \kappa_c) = (0., 0.25)$  already known from strong coupling expansion.

The study of the (gauge invariant) photon plaquette-plaquette correlator  $\Gamma_\gamma(\tau)$  can serve to distinguish between the different phases. In the confinement phase of WA  $\Gamma_\gamma(\tau)$  decays very quickly with increasing  $\tau$ , so that for the photon mass  $m_\gamma$  the conclusion  $m_\gamma > 0$  can be drawn. In the Coulomb phase the behaviour of the correlator is consistent with the expected zero mass behaviour. In the 3rd phase our data also indicate the existence of a massless photon, but still more effort is needed to draw the final conclusion about the photon mass in the two 'upper' phases.<sup>2</sup>

In the following we want to discuss the chiral limit or transition from the Coulomb phase to the higher- $\kappa$  phase(s).

As in the case of the quenched theory the study of the time histories of different observables, in particular,  $\Pi$ , can give a signal of approaching  $\kappa_c$ . However, in the case of the theory with dynamical fermions the fermionic determinant strongly suppresses the small eigenvalues, and there are no such sharp peaks in the time histories as in the case of the quenched theory. Nevertheless, the study of time histories shows that by approaching  $\kappa_c(\beta)$  they become much more noisy than far away from it, testifying the appearance of small eigenvalues of the fermionic matrix  $\mathcal{M}$  (cf. [13]).

Again the statistical variance should be a suitable parameter to express the fluctuations of the observables.

The behaviour of the pion norm  $\langle \Pi \rangle$  and its variance in the full QED is similar to the behaviour of these quantities in the quenched theory.

Fig.8a shows the dependence of  $\langle \Pi \rangle$  on  $\kappa$  at  $\beta = 1.1$  for the standard Wilson action. One can see that the pion norm has a pronounced maximum whose position and value practically does not depend on the lattice size at large enough  $L$  ( $L = 8$  and  $12$  in our case). At smaller values of  $L$  there is still a finite volume dependence. For comparison we show the data points (crosses) for  $\langle \Pi \rangle$  at the same values of  $\beta$  and  $\kappa$ , but for a quenched simulation on a  $8^4$  lattice – this illustrates the influence of the vacuum polarization effects caused by dynamical fermions.

---

<sup>2</sup>In our preliminary publication [5] we conjectured a tachyonic behaviour, i.e.  $m_\gamma^2 < 0$ , in the 3rd phase.

For the variance  $\sigma^2(\Pi)$  of the pion norm (Fig. 8b) the signal in the full QED case is not as strong as in the quenched theory (smaller by a factor of  $\sim 6$ ), because of the effect of the fermionic determinant. Nevertheless, the maximum of the variance  $\sigma^2(\Pi)$  of the pion norm shows a steady growth with increasing  $L$ . (We expect the errorbars shown in the figure to be somewhat underestimated (at most  $\sim 15\%$ ) since we have seen strong autocorrelations in our data for  $\sigma^2(\Pi)$ , especially around  $\kappa_c$ .) We also observe a shift of the maximum of  $\sigma^2(\Pi)$  'to the left' the more  $L$  is increased. Therefore, the variance of the pion norm seems to exhibit the characteristic features of a finite size scaling behaviour of a singular point on finite volume systems.

We are led to the conclusion, that a chiral phase transition in the thermodynamic sense really exists. We might speculate that the corresponding singularity appears to be rather 'weak', i.e., other operators and their fluctuations, like the fermionic condensates and the plaquette operator do not show a singular behaviour, as far as we can tell for the given lattice sizes. As the variance of the pion norm itself can be interpreted as a higher derivative operator we speculate that the singularity may be viewed as a higher order phase transition.

Based on our observations we conclude that the variance of the pion norm  $\sigma^2(\Pi)$  is a convenient 'order parameter' for determining the position of the chiral transition in the Coulomb phase. On the other hand the average pion norm itself, its time histories and  $\langle N_{cg}^{-1} \rangle$  can provide estimates of  $\kappa_c$ .

Turning to the investigation of the phase structure of the theory MA (eq.(4)) the situation drastically changes in comparison with the standard theory WA. Similarly to the quenched theory in the full QED with artifacts suppressed we see only one phase at  $\kappa < \kappa_c(\beta)$ , and only one unique phase just above the line  $\kappa_c(\beta)$ . Moreover, we do not observe metastable states when crossing the 'horizontal' line, and no hysteresis shows up in thermal cycles. The average plaquette and the fermionic condensate, respectively, turn out to behave smoothly with varying  $\kappa$  at fixed  $\beta$ . This has been checked for  $\beta = 0$  and  $\beta = 1.1$ . The corresponding curves look very similar. So, there is no sign for a first order transition.

We have also explored the small  $\beta$ -region of the phase diagram above the chiral phase transition  $\kappa_c(\beta)$  in the standard Wilson action formulation. As it was already noted strong coupling arguments suggest for  $\beta = 0$  and for  $\kappa$ -values above  $\kappa_c(\beta = 0) = 0.25$  the existence of zero eigenvalues of the fermion matrix. It is a valid question how this singularity is approached in the dynamical fermion simulation for positive values of  $\beta$ , and for  $\kappa > \kappa_c(\beta)$ , i.e. above the chiral phase transition line. In particular one might ask whether this singularity of the theory extends to finite  $\beta$ -values and whether a corresponding unphysical phase of the theory exists.

We have simulated the approach to small  $\beta$ -values at a fixed Wilson coupling value  $\kappa = 0.3 > \kappa_c(\beta)$  on a  $4^4$  lattice for various  $\beta$ -values in runs of 1000 measurements, i.e. 4000 trajectories.

In this region of the phase diagram we encountered acceptance rate problems in the Hybrid Monte Carlo algorithm. For this reason we have decreased the step-

size  $\delta\tau$  to 0.025 while keeping the trajectory length fixed at unity – the resulting acceptance rate turned out to be about 84 %.

With decreasing  $\beta$  we observe a rapid increase of the number of the conjugate gradient steps  $N_{cg}$  needed for the fermion matrix inversion (Fig.9a). A linear extrapolation of the average inverse number  $\langle N_{cg}^{-1} \rangle \rightarrow 0$  of conjugate gradient steps (dotted line in Fig.9a) can be consistent with a singular point around  $\beta \sim 0.15$ .

In Fig.9b we display the time evolution of the pion norm  $\Pi$  at decreasing values of  $\beta$ . The more  $\beta$  is lowered the more sharp spikes with increasing amplitude are observed in the time evolution of the operator, similar to that in the quenched theory (compare with Fig.3). The appearance of such spikes makes it practically impossible to calculate a statistically reliable average value.

We therefore conclude that the point  $\beta \sim 0.15$  at  $\kappa = 0.3$  is part of a singular line  $\beta = \beta(\kappa), \kappa > 0.25$  which separates the 4th from the 3rd phase.

The 4th phase could be expected to be a parity–violating phase (see [30]). In case of QCD the existence of a parity violating–phase for  $\kappa > \kappa_c(\beta)$  was numerically based on the behaviour of the fluctuation of the pseudoscalar density  $\langle \bar{\psi}\gamma_5\psi \rangle$  [31]. We studied the distribution of  $\bar{\psi}\gamma_5\psi$  at  $(\beta = 0; \kappa < \kappa_c)$  and  $(\beta = 0; \kappa > \kappa_c)$  in order to find a signal for parity–violation in the quenched approximation of the standard Wilson action on a  $4^4$  lattice. The distribution width increases roughly by a factor of 6 while crossing  $\kappa_c$  from below. This is due to the appearance of small eigenvalues of  $\mathcal{M}$  for  $\kappa > \kappa_c$  leading to large fluctuations of  $\bar{\psi}\gamma_5\psi$  seen as spikes in the time history. The shape of the distribution does not change, especially we do not find any double–peak structure for  $\kappa > \kappa_c$ . One has to repeat this analysis on a larger lattice to control the finite size effects. Preliminary our data do not show parity–violation for the considered  $(\beta, \kappa)$ –values.

The phase diagrams for both theories (with standard gauge action and with modified action) are shown in Figs.10a,b. For the standard action WA (Fig.10a) we show four different phases at  $\kappa \lesssim 0.3$ , whereas for the modified theory MA only two phases survive in the same  $\kappa$ –range (Fig10b).

## 6 Conclusions and Outlook

Now let us summarize our results.

- We have studied the phase structure of two theories with Wilson fermions and compact action with  $U(1)$  symmetry : standard Wilson theory and a modified one with lattice artifacts suppressed. Phase diagrams of both theories were shown.
- For the standard Wilson theory there is a 'horizontal' line  $\kappa_c(\beta)$  from a  $(\beta_1; \kappa_1)$  to  $(\infty; \frac{1}{8})$  which separates the Coulomb phase from the 3rd phase and which corresponds to the *chiral transition* in this theory. Presumably, a higher order phase transition occurs on this line. At smaller values of  $\beta$  ( $\beta < \beta_1$ )

on the continuation of this line we find a presumably first order chiral phase transition.

- When suppressing the lattice artifacts the latter 1st order phase transition disappears.
- Nevertheless, after suppressing the lattice artifacts a chiral transition (i.e., appearance of near-to-zero eigenvalues of  $\mathcal{M}$ ) remains for all  $\beta$  values we considered. The statistical variance of the pion norm gives us a pronounced signal for both (quenched and dynamical) cases. Its location turned out to be in reasonable agreement with that obtained from the cg-method (measuring  $\langle N_{cg}^{-1} \rangle$ ).
- The behaviour of all considered gauge-invariant observables *along* the critical line  $\kappa_c(\beta)$  in the Coulomb phase is smooth. Thus, for the modified action, we have no indication for a (tri-) critical point on this line, in contrast to lattice QED with staggered fermions and the non-compact gauge action.
- The calculation of the (gauge-variant) fermionic propagator needs a gauge-fixing procedure which can appear to be rather nontrivial because of gauge fixing ambiguities [6]. In a recent paper [7], some of the gauge copies were shown to produce a photon propagator with a decay behaviour inconsistent with the expected zero mass behaviour in the Coulomb phase. In Ref. [8] it was proven that the "bad" gauge copies are due to the existence of pairs of *Dirac sheets* as gauge artifacts. For matter fields to be taken into account this problem requires additional studies before one can reliably compute fermionic correlators.
- As a further step we plan to investigate the spectra of both theories and to determine renormalized quantities such as the renormalized coupling.

## Acknowledgements

We would like to acknowledge useful discussions with E. Laermann, P. Rakow, G. Schierholz, R. Sommer and U.-J. Wiese.

## Figure captions.

**Fig.1** The average residue  $\langle R \rangle$  as a function of  $N_{cg}$  for gaussian distribution of eigenvalues  $\lambda_i$  of the hermitian matrix  $D$  in the interval  $[\lambda_{min}; \lambda_{max}]$ . Broken lines correspond to the behaviour  $\exp(-\alpha \cdot N_{cg})$  where  $\alpha$  is defined in eq.(15).

**Fig.2a** The dependence of  $\langle N_{cg}^{-1} \rangle$  on  $\kappa$  at  $\beta = 1.1$  for the quenched Wilson action (qWA) and different lattice sizes  $L$ . The broken line has been added to guide the eye.

**Figs.2b,c**  $\langle N_{cg}^{-1} \rangle$  as a function of the inverse lattice size  $L^{-1}$  at different values of  $\kappa$  for **(b)** qWA at  $\beta = 1.1$  and **(c)** the quenched modified action (qMA) at  $\beta = 0.8$ . Broken lines are to guide the eye.

**Fig.3** Time histories of  $\Pi$  at different  $\kappa$  at  $\beta = 0$  for qWA.

**Fig.4** Time histories of  $\Pi$  at different  $\kappa$  at  $\beta = 1.1$  for qWA.

**Figs.5a,b**  $\sigma^2(\Pi)$  as a function of  $\kappa$  for qWA at  $\beta = 1.1$  **(a)** and the qMA at  $\beta = 0$  **(b)**. The broken lines indicate the maxima of  $\sigma^2(\Pi)$ .

**Fig.6** Distribution functions of the plaquette operator without (dots) and with (crosses) suppression term (19) at  $\beta = 0.8$ ,  $\kappa = 0.1$  on a  $6^4$  lattice.

**Figs.7a,b** The thermal cycle for  $\bar{\psi}\psi$  **(a)** and for the monopole density  $\rho_{mon.}$  **(b)** with respect to  $\kappa$  at  $\beta = 0.8$  for WA with dynamical fermions on a  $6^4$  lattice.

**Figs.8a,b** Average pion norm  $\langle \Pi \rangle$  **(a)** and  $\sigma^2(\Pi)$  **(b)** as a function of  $\kappa$  for WA at  $\beta = 1.1$ . Lattice size is  $4^4$  (circles),  $6^4$  (squares),  $8^4$  (diamonds) and  $12^4$  (triangles). For comparison the data from a quenched simulation on a  $8^4$  lattice is shown (crosses) in Fig.8a.

**Figs.9a,b**  $\langle N_{cg}^{-1} \rangle$  as a function of  $\beta$  at  $\kappa = 0.3$  **(a)** and time histories of  $\Pi$  at  $\kappa = 0.3$  and different  $\beta$  **(b)** for WA on a  $4^4$  lattice.

**Figs.10a,b** Phase diagram in the  $(\beta, \kappa)$ -plane for dynamical fermions for the standard Wilson action WA **(a)** and for the modified action MA **(b)**.

## References

- [1] K. Wilson, Phys. Rev. **D10** (1974) 2445; in New phenomena in subnuclear physics, ed. A. Zichichi (Plenum, New York, 1977)
- [2] M. Lüscher, Comm. Math. Phys. 54 (1977) 283
- [3] N. Kawamoto, Nucl. Phys. **B190** (1981) 617
- [4] N. Kawamoto and J. Smit, Nucl. Phys. **B192** (1981) 100

- [5] A. Hoferichter, V.K. Mitrjushkin, M. Müller–Preussker and Th. Neuhaus, Nucl.Phys. **B** (Proc. Suppl.) 34 (1994) 537
- [6] V.N. Gribov, Nucl. Phys. **B139** (1978) 1
- [7] A. Nakamura and M. Plewnia, Phys. Lett. **255B** (1991) 274
- [8] V.G. Bornyakov, V.K. Mitrjushkin, M. Müller-Preussker and F.Pahl, Phys. Lett. **B317** (1993) 596
- [9] T.A. DeGrand and D. Toussaint, Phys. Rev. **D22** (1980) 2478
- [10] J. S. Barber, R. E. Shrock and R. Schrader, Phys. Lett. **B152** (1985) 221  
J. S. Barber and R. E. Shrock, Nucl. Phys. **B257** [FS 14] (1985) 515
- [11] V.G. Bornyakov, V.K. Mitrjushkin and M. Müller–Preussker, Nucl. Phys. **B** (Proc. Suppl.) 30 (1993) 587
- [12] A. Hoferichter, V.K. Mitrjushkin and M. Müller–Preussker, HU Berlin–IEP–94/11, hep-lat/9407009
- [13] K. Bitar, A. D. Kennedy and P. Rossi, Phys. Lett. **B234** (1990) 333
- [14] S. Itoh, Y. Iwasaki and T. Yoshié, Phys. Rev. **D36** (1987) 527
- [15] I. Barbour, E. Laermann, Th. Lippert and K. Schilling, Phys. Rev. **D46** (1992) 3618
- [16] A. Ukawa, CERN-TH-5245/88 (1988)
- [17] A. Nakamura and R. Sinclair, Phys. Lett. **243B** (1990) 396
- [18] B. Berg and C. Panagiotakopoulos, Phys. Rev. Lett. **52** (1984) 94
- [19] M. R. Hestenes and E. Stiefel, Journal of Research of the NBS **49** (1952) 409
- [20] M. Engeli et al., *Mitteilungen aus dem Institut für angewandte Mathematik* (Birkhäuser Verlag, Berlin, 1959), Vol. 8, p. 24
- [21] A. Nakamura, G. Feuer, H.C. Hege and V. Linke, Comp. Phys. Comm. **51** (1988) 301
- [22] Th. A. DeGrand, Comp. Phys. Comm. **52** (1988) 161
- [23] Th. A. DeGrand and P. Rossi, Comp. Phys. Comm. **60** (1990) 211
- [24] A. Cornelius, thesis Hamburg University (1991), unpublished
- [25] G. Schierholz, Nucl. Phys. **B** (Proc. Suppl.) 20 (1991) 623

- [26] S. Duane, A. D. Kennedy, B. J. Pendleton and D. Roweth,  
Phys. Lett. **B195** (1987) 216
- [27] C. Hege and A. Nakamura, Nucl. Phys. **B** (Proc. Suppl.) 9 (1989) 114
- [28] C.B. Lang and T. Neuhaus, Nucl. Phys. **B** (Proc. Suppl.) 34 (1994) 543;  
C.B. Lang and T. Neuhaus, BI-TP 94/37, hep-lat/9407005
- [29] M. Baig and H. Fort, UAB-FT-338
- [30] S. Aoki, Phys. Rev. **D30** (1984) 2653
- [31] S. Aoki, Phys. Lett. **B190** (1987) 140

This figure "fig1-1.png" is available in "png" format from:

<http://arxiv.org/ps/hep-lat/9408014v1>

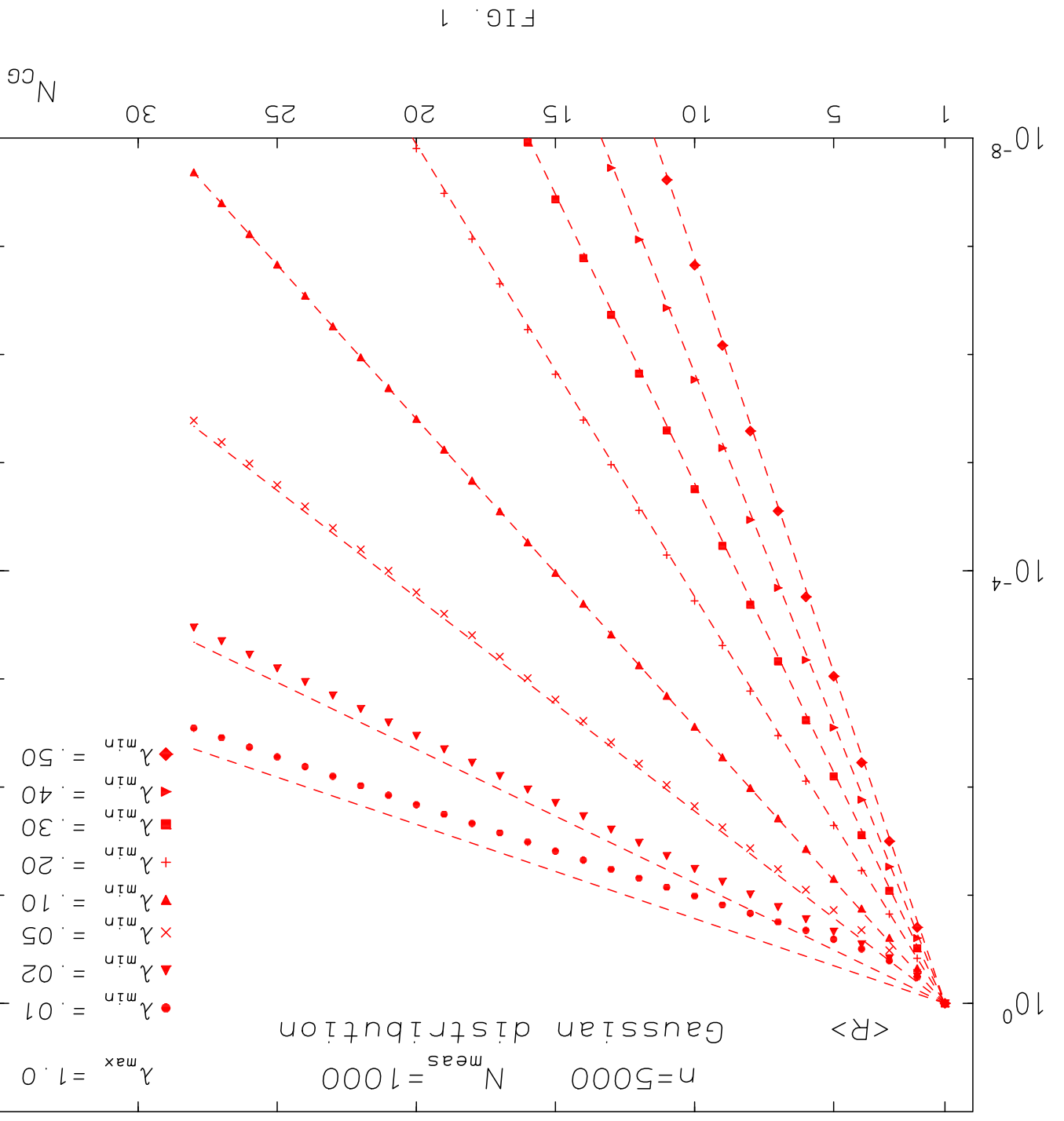


FIG. 1

This figure "fig2-1.png" is available in "png" format from:

<http://arxiv.org/ps/hep-lat/9408014v1>

This figure "fig3-1.png" is available in "png" format from:

<http://arxiv.org/ps/hep-lat/9408014v1>

This figure "fig1-2.png" is available in "png" format from:

<http://arxiv.org/ps/hep-lat/9408014v1>

This figure "fig2-2.png" is available in "png" format from:

<http://arxiv.org/ps/hep-lat/9408014v1>

FIG. 2a

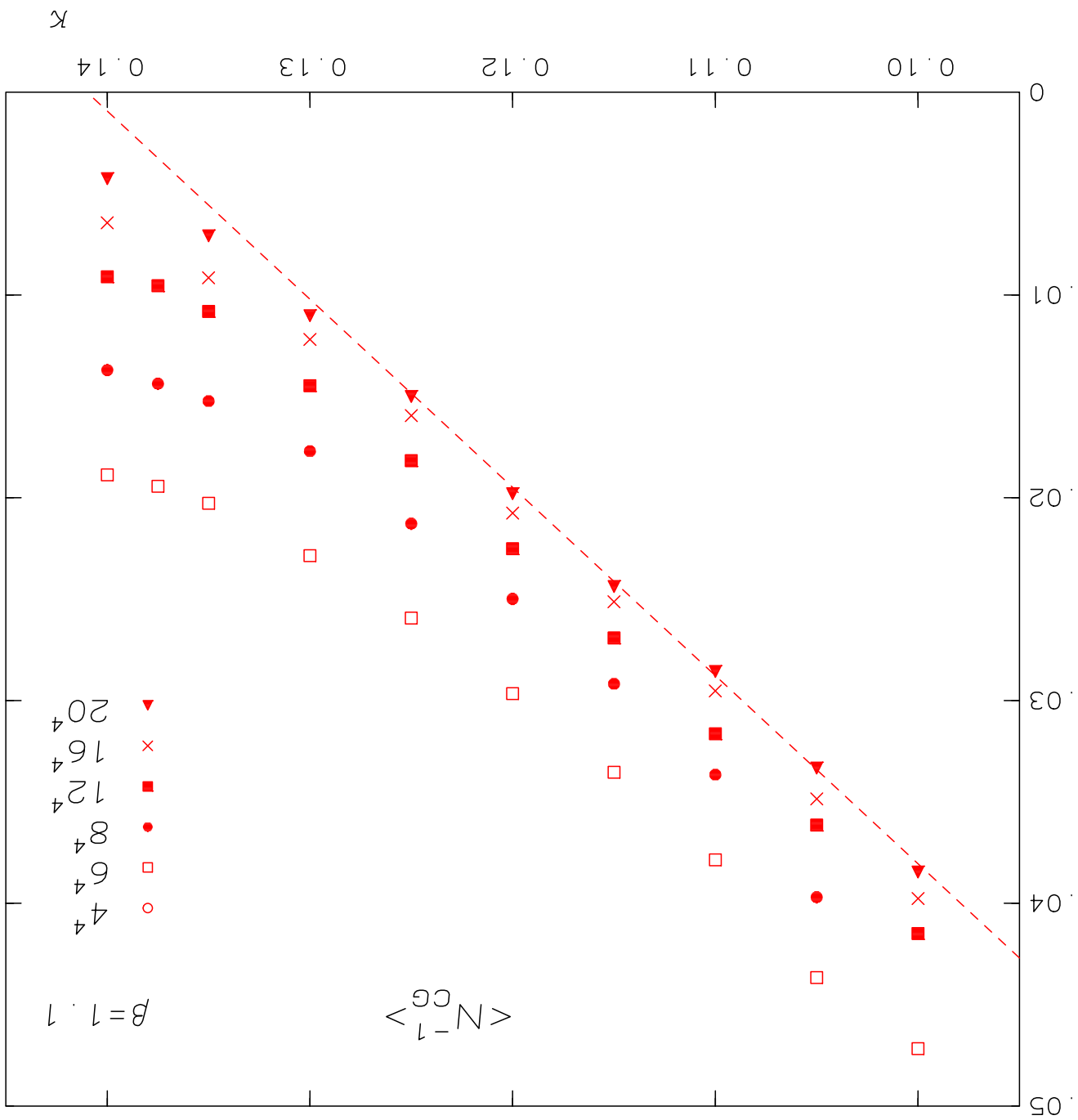
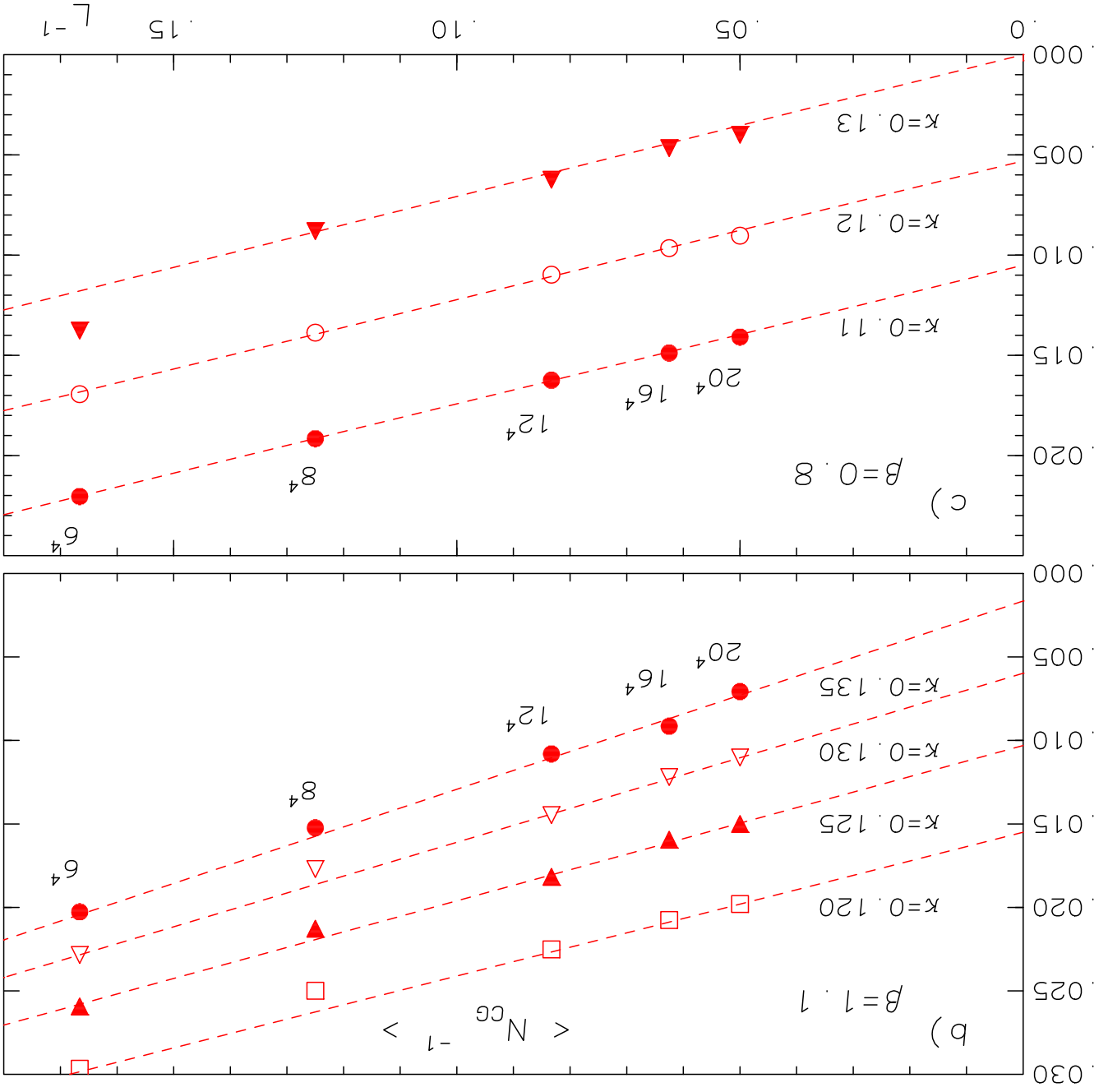


FIG. 2b,c



This figure "fig3-2.png" is available in "png" format from:

<http://arxiv.org/ps/hep-lat/9408014v1>

This figure "fig1-3.png" is available in "png" format from:

<http://arxiv.org/ps/hep-lat/9408014v1>

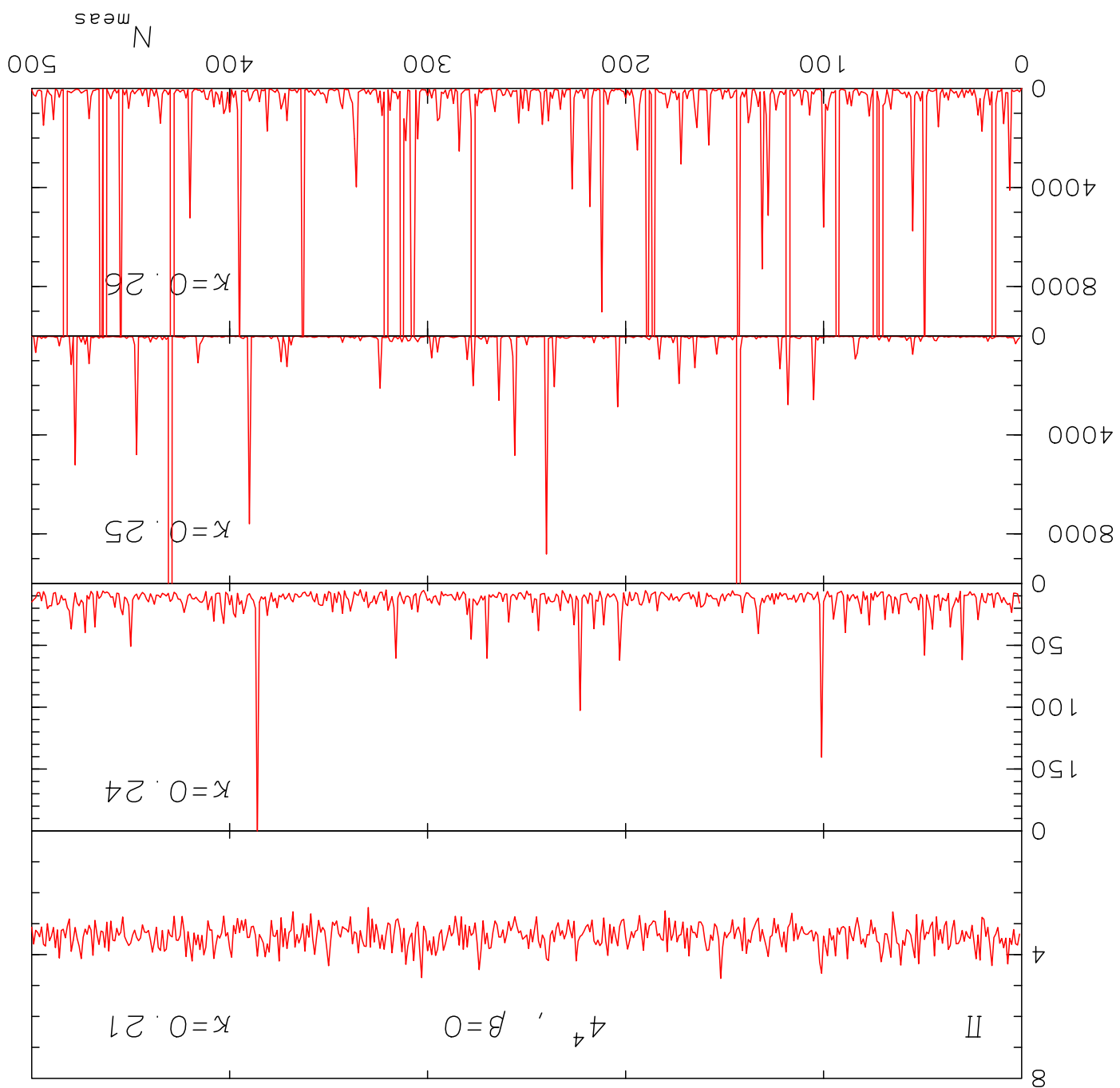
This figure "fig2-3.png" is available in "png" format from:

<http://arxiv.org/ps/hep-lat/9408014v1>

This figure "fig3-3.png" is available in "png" format from:

<http://arxiv.org/ps/hep-lat/9408014v1>

FIG. 3



This figure "fig1-4.png" is available in "png" format from:

<http://arxiv.org/ps/hep-lat/9408014v1>

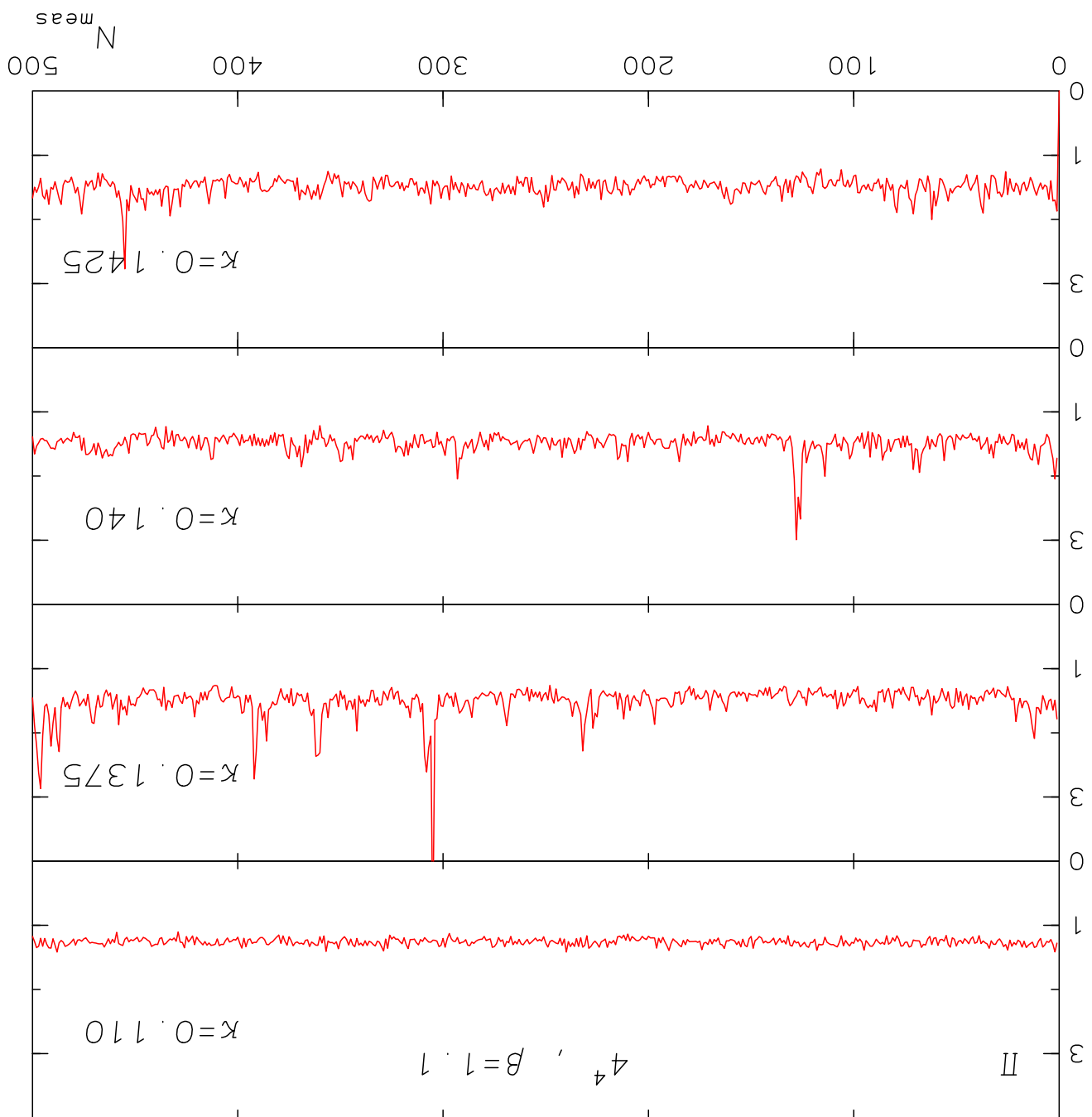
This figure "fig2-4.png" is available in "png" format from:

<http://arxiv.org/ps/hep-lat/9408014v1>

This figure "fig3-4.png" is available in "png" format from:

<http://arxiv.org/ps/hep-lat/9408014v1>

FIG. 4



This figure "fig1-5.png" is available in "png" format from:

<http://arxiv.org/ps/hep-lat/9408014v1>

FIG. 5a,b

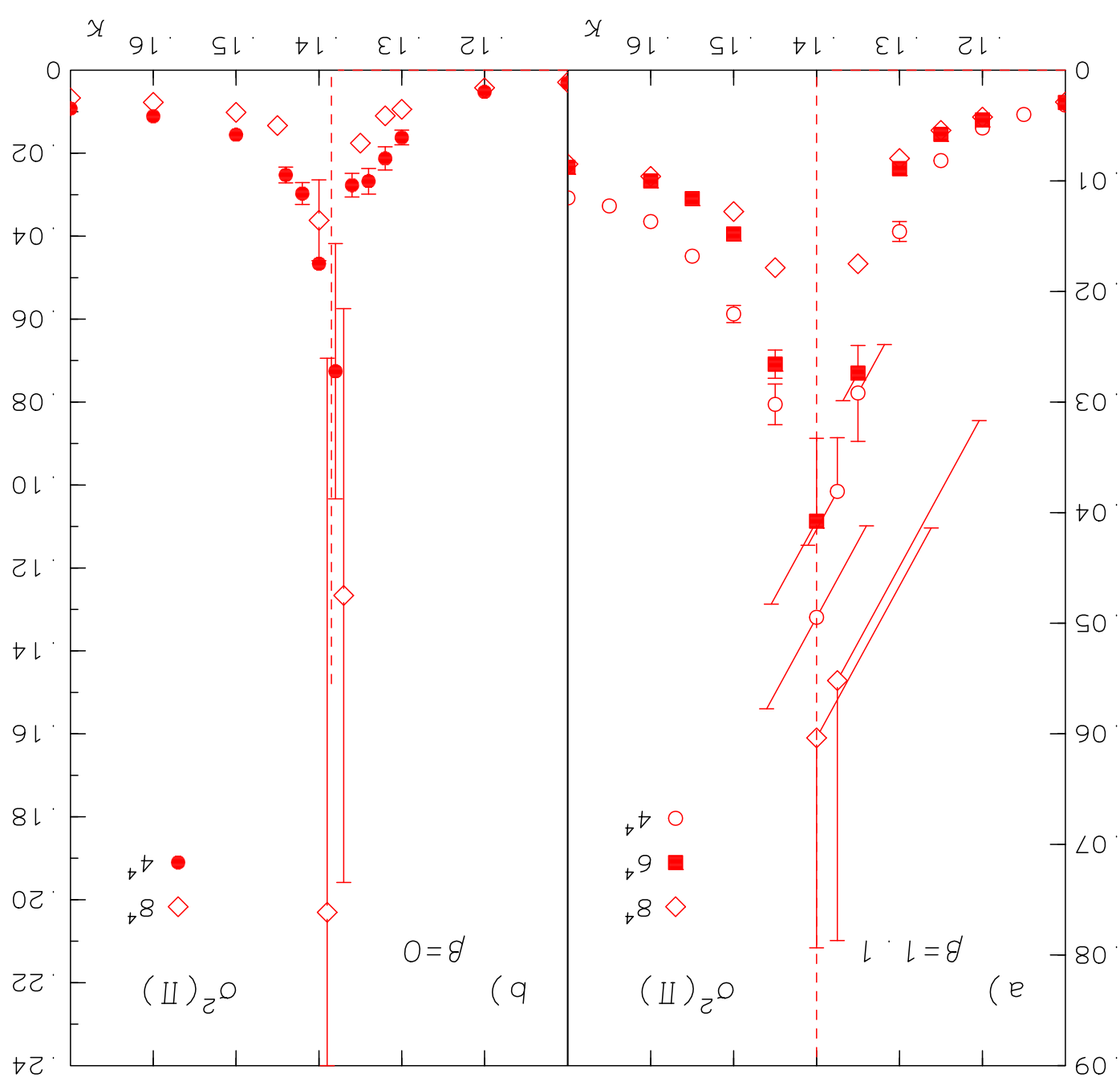


FIG. 6

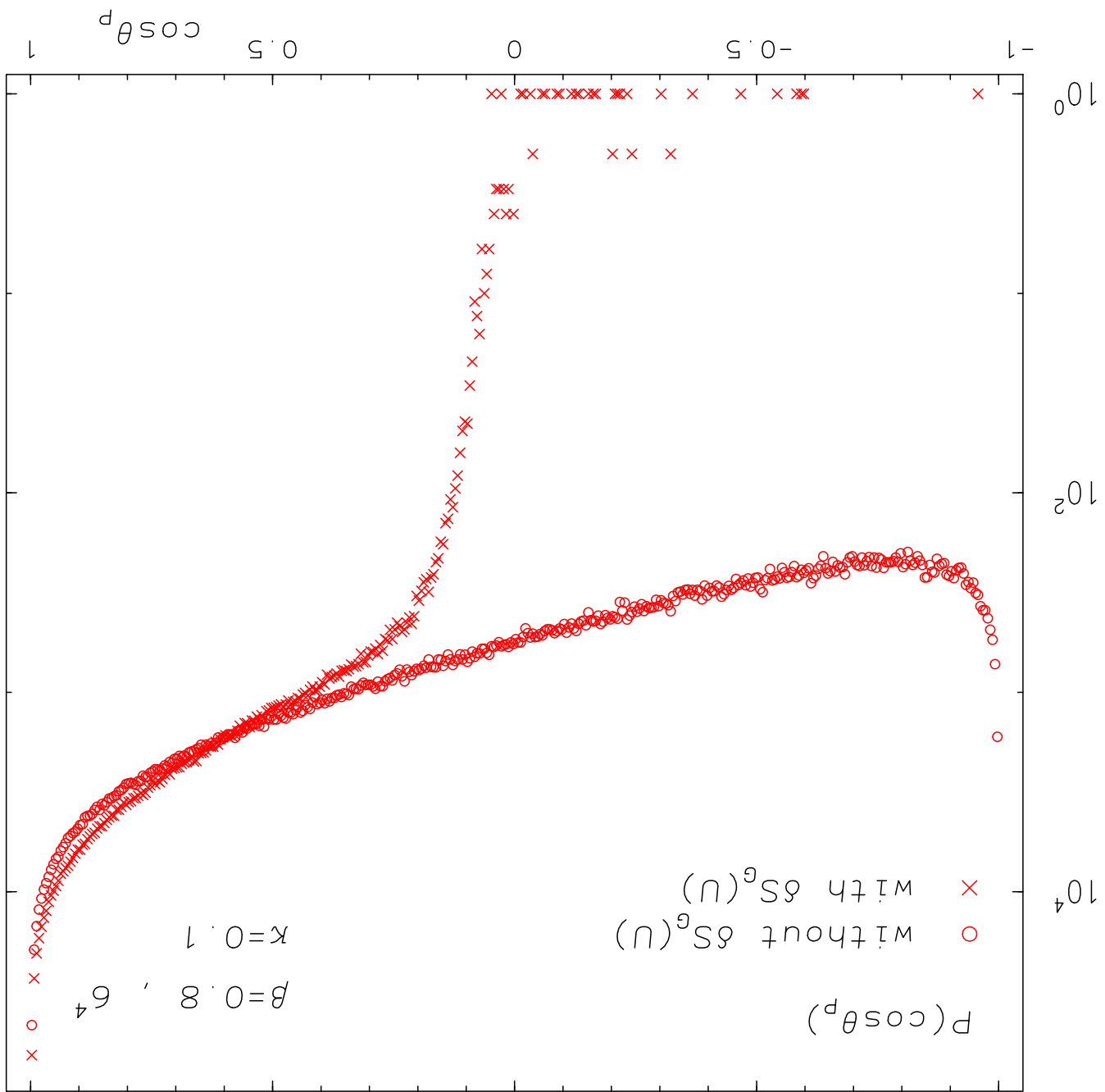


FIG. 7a

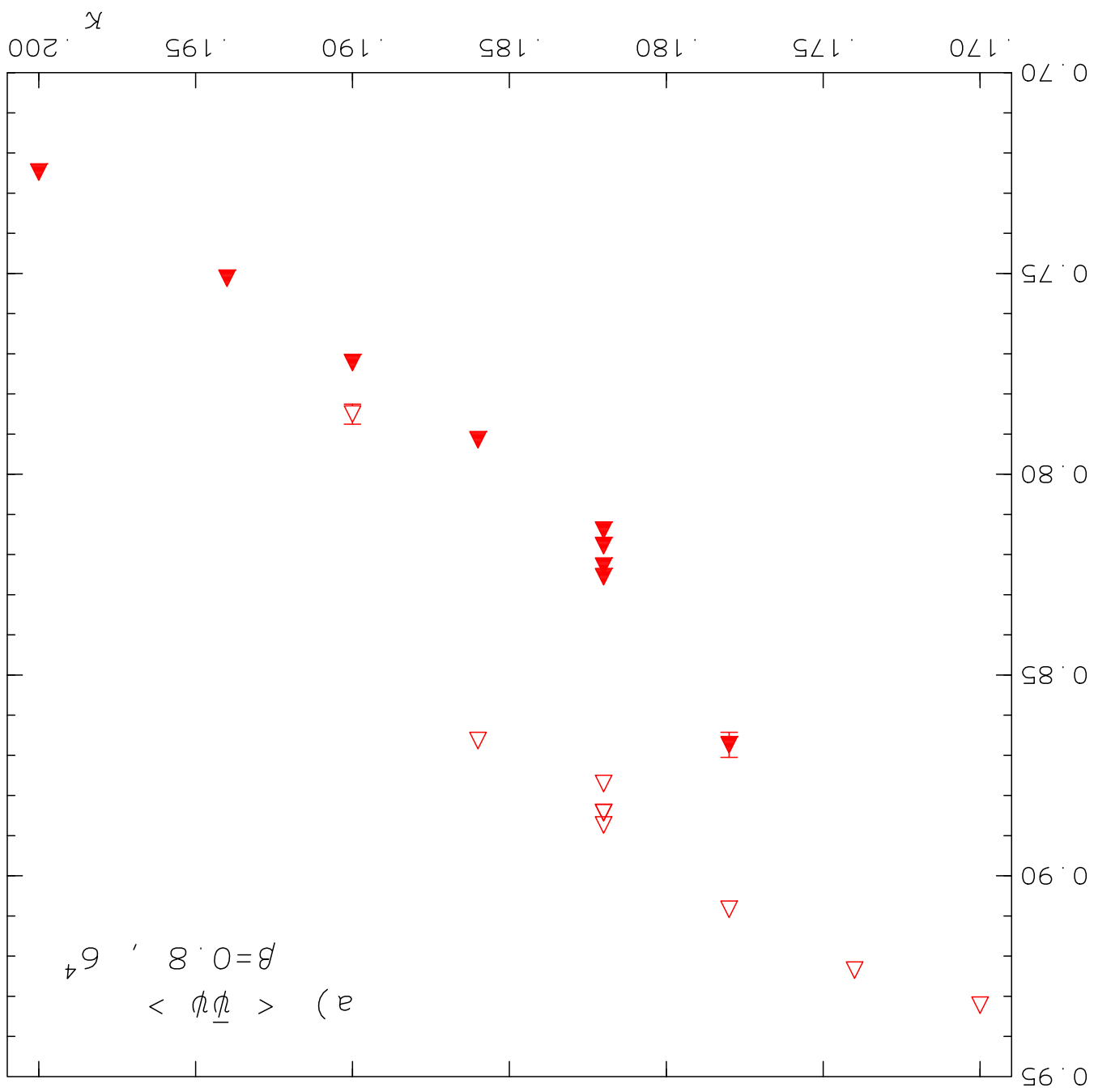


FIG. 7b

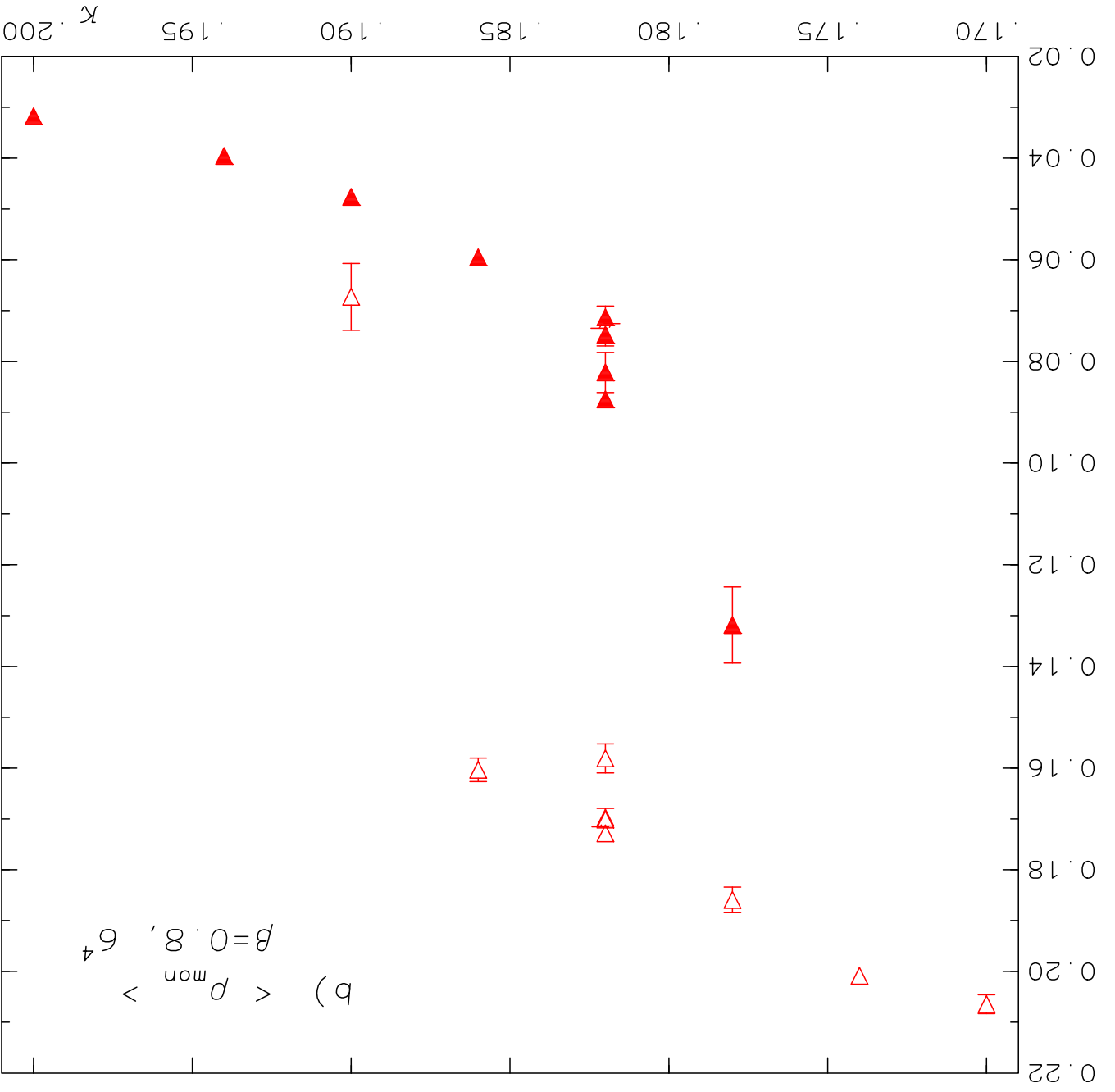


FIG. 8a

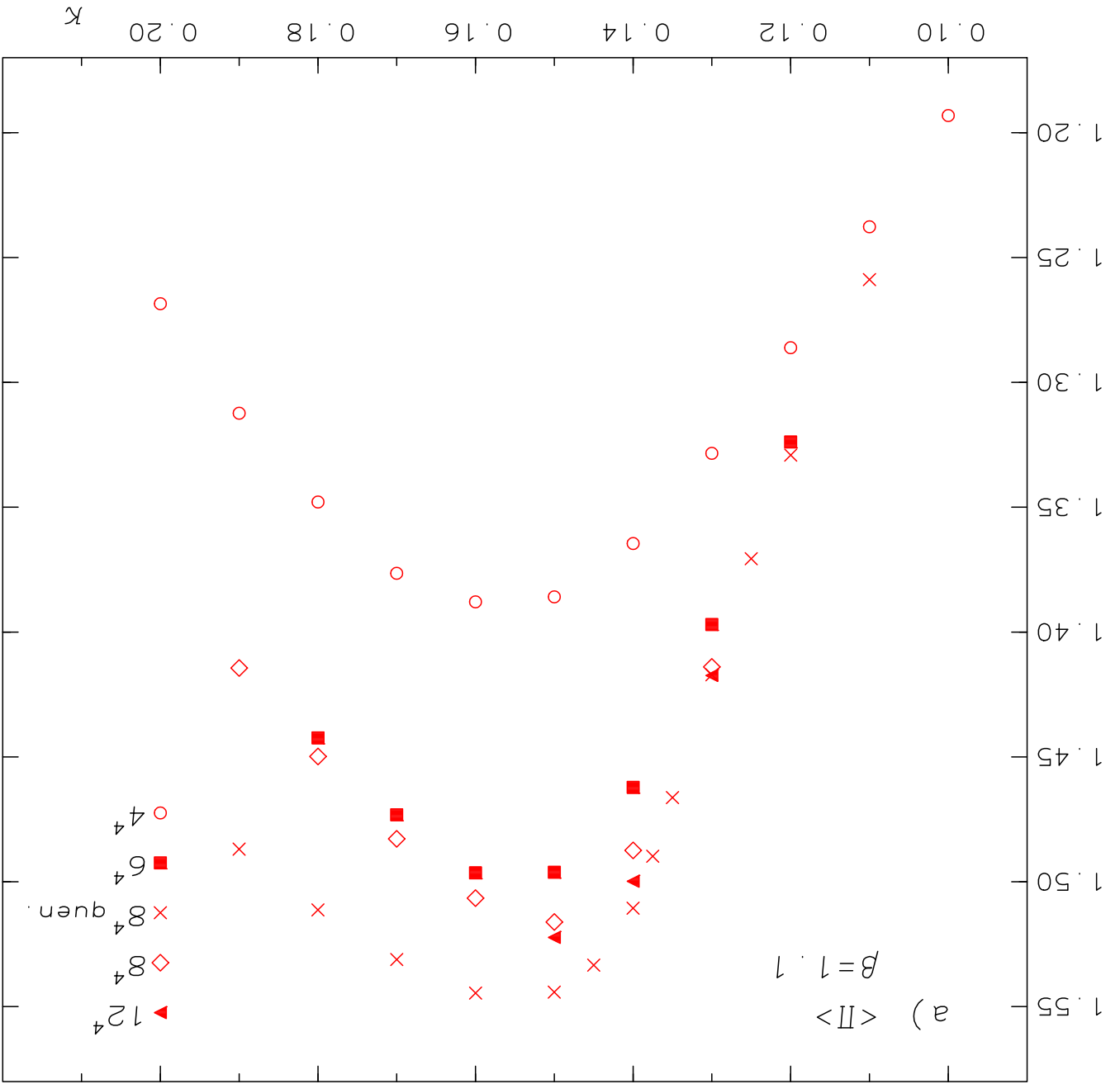


FIG. 8b

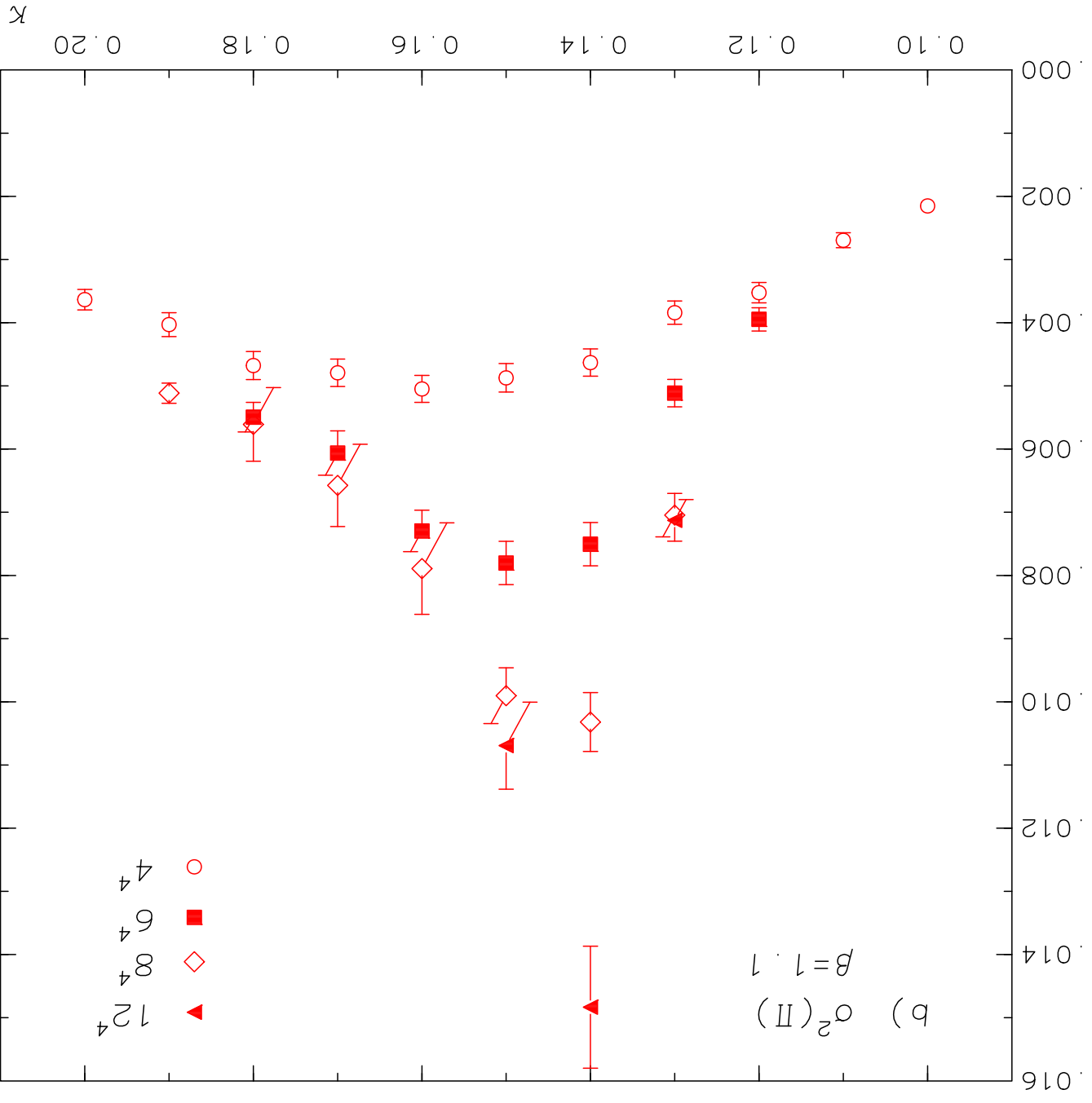


FIG. 9a

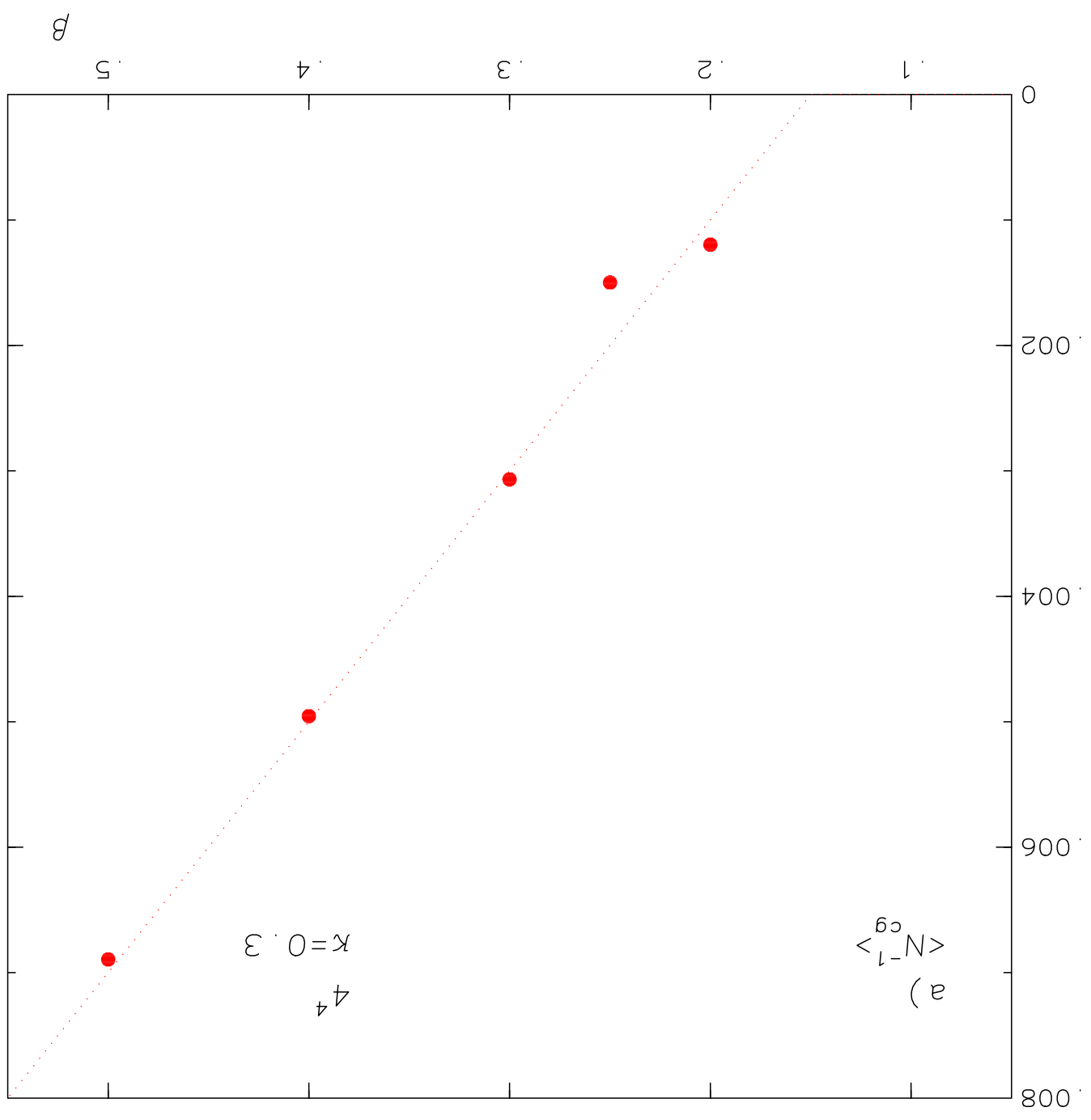


FIG. 9b

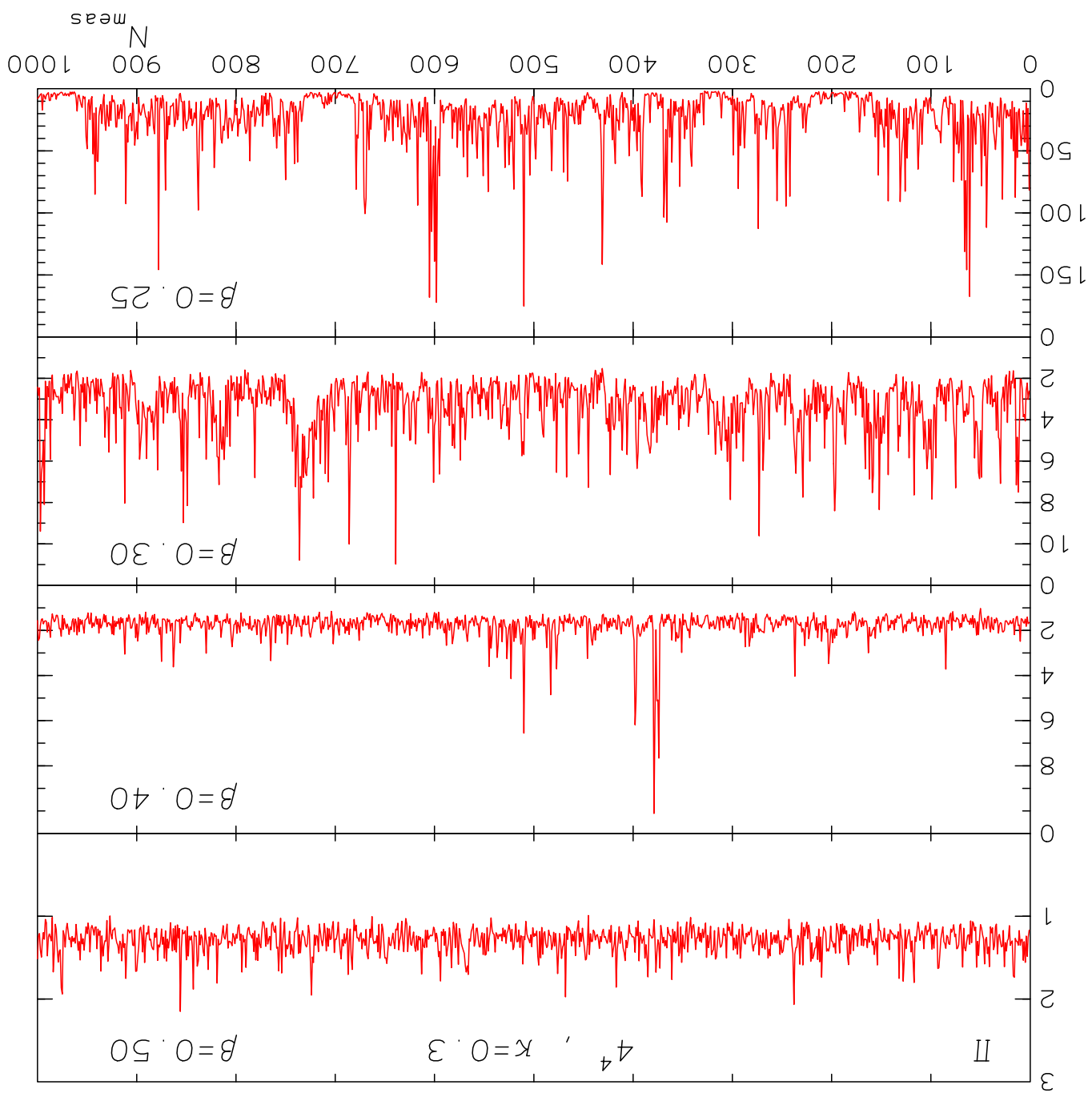


FIG. 10a,b

